International Journal of Heat and Mass Transfer 83 (2015) 327–336

Contents lists available at ScienceDirect

International Journal of Heat and Mass Transfer

journal homepage: www.elsevier.com/locate/ijhmt

Local thermal non-equilibrium analysis of the thermoconvective instability in an inclined porous layer

A. Barletta [a,*], D.A.S. Rees [b]

[a] Department of Industrial Engineering, Alma Mater Studiorum Università di Bologna, Viale Risorgimento 2, Bologna 40136, Italy
[b] Department of Mechanical Engineering, University of Bath, Claverton Down, Bath BA2 7AY, UK

ARTICLE INFO

Article history:
Received 26 October 2014
Accepted 1 December 2014

Keywords:
Porous medium
Darcy's law
Linear stability
Inclined layer
Local thermal non-equilibrium

ABSTRACT

The two-temperature model of local thermal non-equilibrium (LTNE) is employed to investigate the onset of secondary convective flow in a fluid-saturated porous layer inclined to the horizontal and heated from below. The layer is assumed to be bounded by impermeable plane parallel walls with uniform and unequal temperatures. The linear instability of the stationary pure-conduction single-cell basic flow is studied by employing a normal mode decomposition of the disturbances. A Squire-like transformation is adopted to map all the oblique roll modes onto equivalent transverse roll modes. It is shown that the longitudinal rolls are the most unstable modes at the onset of the instability. The neutral stability condition for the longitudinal modes corresponds to that for a horizontal layer, by scaling the Darcy–Rayleigh number with cosine of the inclination angle to the horizontal. This scaling law, coincident with that well-known for the local thermal equilibrium (LTE) regime, implies a monotonic increment in the stability of the basic flow as the inclination to the horizontal increases.

1. Introduction

The study of the onset of thermal instability in a saturated porous layer heated from below is a classical problem in convection heat transfer. This topic deserved a wide space in the literature of the last decades, and it has been reported in many books and review papers such as Nield and Bejan [1], Rees [2], Tyvand [3] and Barletta [4]. A special focus has been made by several authors on the case where a plane porous layer is inclined to the horizontal and bounded by impermeable isothermal walls. A temperature difference between the walls may lead to an unstable stratification that, however, has a nature different from that of a horizontal layer, *viz.* the usual Darcy–Bénard setup [2]. In fact, the inclination to the horizontal results in a basic stationary state where the fluid is not at rest, but circulates along a single cell of infinite width. Strictly speaking, the basic velocity field is parallel, bidirectional, and with a vanishing mass flow rate.

Among the first investigators of the inclined layer instability, we mention Bories and Combarnous [5], Weber [6], Caltagirone and Bories [7]. The main effect of the inclination is that the onset of the thermal instability is with a critical Darcy–Rayleigh number given by $4\pi^2/\cos\phi$, where ϕ is the inclination angle of the layer to the horizontal. In other words, for the onset of the linear instability, a simple scaling law with respect to the Darcy–Bénard problem for a horizontal layer was proved [1]. Further results on the stability of an inclined porous layer were obtained by Storesletten and Tveitereid [8], Karimi-Fard et al. [9], Rees and Bassom [10], and Rees et al. [11]. Karimi-Fard et al. [9] carried out an investigation of oscillatory instability for the case of double-diffusion. Rees and Bassom [10] defined a Squire-like transformation allowing a general study of normal modes with an arbitrary orientation. Storesletten and Tveitereid [8] included in the stability analysis the effect of anisotropy in the porous medium, while Rees et al. [11] extended this analysis by considering an arbitrary orientation of the principal axes of anisotropy.

A recent note by Nield [12] contains new insights into the question of the preferred patterns at the onset of the instability: rolls or polyhedral cells. Nield et al. [13] investigated the influence of the viscous dissipation effect on the onset of instability in an inclined layer. Uniform heat flux boundary conditions, as possible models of the heating from below, were considered in the stability analyses of the inclined porous layer carried out by Barletta and Storesletten [14] and by Rees and Barletta [15].

The aim of this paper is to revisit the topic of instability in an inclined porous layer, by relaxing the assumption that the solid phase and the fluid phase are in local thermal equilibrium (LTE).

* Corresponding author.
E-mail addresses: antonio.barletta@unibo.it (A. Barletta), ensdasr@bath.ac.uk (D.A.S. Rees).

http://dx.doi.org/10.1016/j.ijheatmasstransfer.2014.12.006
0017-9310/

Nomenclature

a	dimensionless wave number
a_x; a_z	components of the dimensionless wave vector
c	specific heat
$\hat{\mathbf{e}}_x$; $\hat{\mathbf{e}}_y$; $\hat{\mathbf{e}}_z$	unit vectors in the (x,y,z)−directions
$\mathbf{g}$; g	gravitational acceleration; modulus of $\mathbf{g}$
h	inter-phase heat transfer coefficient
H	dimensionless inter-phase heat transfer parameter, Eq. (2)
k	thermal conductivity
k_m	effective thermal conductivity, $\chi k_f + (1-\chi)k_s$
K	permeability
L	layer thickness
LTE	local thermal equilibrium
LTNE	local thermal non-equilibrium
p	dimensionless pressure disturbance amplitude, Eq. (10)
P	dimensionless pressure disturbances, Eq. (8)
R	Darcy–Rayleigh number, Eq. (2)
$\Re e$; $\Im m$	real part; imaginary part
S; $\tilde{S}$	transformed Darcy–Rayleigh numbers, Eqs. (12) and (22)
t	dimensionless time, Eq. (2)
$T_{s,f}$	dimensionless temperatures, Eq. (2)
$\mathbf{u}$	dimensionless velocity, (u,v,w), Eq. (2)
$\mathbf{U}$	dimensionless velocity disturbance, (U,V,W), Eq. (5)
$\mathbf{x}$	dimensionless position vector, (x,y,z), Eq. (2)

Greek symbols

α	thermal diffusivity
α_m	effective thermal diffusivity, $k_m/(\rho c)_f$
β	thermal expansion coefficient
γ	dimensionless parameter, Eq. (2)
ΔT	reference temperature difference
ε	dimensionless perturbation parameter, Eq. (5)
$\eta_{1...4}$	real dimensionless parameters, Eq. (B1)
θ	average dimensionless temperature, Eq. (27)
$\theta_{s,f}$	dimensionless temperature disturbance amplitudes, Eq. (10)
$\Theta_{s,f}$	dimensionless temperature disturbances, Eq. (5)
λ	dimensionless parameter, Eq. (2)
$\Lambda_c(\Phi)$	dimensionless function, Eq. (31)
ν	kinematic viscosity
ρ	density
φ	porosity
ϕ	inclination angle to the horizontal
Φ	transformed angle, Eq. (12)
χ	porosity
ω	complex dimensionless parameter, Eq. (10)

Superscript, subscripts

$\bar{}$	complex conjugate
$\star$	dimensional quantity
b	basic solution
c	critical value
f	fluid phase
s	solid phase
$'$	differentiation with respect to y

Thus, a two-temperature model will be adopted to describe, through a finite inter-phase heat transfer coefficient, the condition of local thermal non-equilibrium (LTNE) [1,16–31]. The study described in this paper is to be considered as a generalisation of the LTNE stability analysis, relative to the Darcy–Bénard problem and hence to a horizontal layer, presented in the paper by Banu and Rees [21].

2. Mathematical model

Let us consider an inclined porous layer saturated by a fluid. We denote as $\phi \in [0^\circ, 90^\circ]$ the inclination angle to the horizontal. The boundary planes, $y^\star = 0, L$, are assumed to be impermeable and isothermal with different temperatures: $T_0 + \Delta T$ is the temperature of the lower boundary, while T_0 is the temperature of the upper boundary, with $\Delta T > 0$. A sketch of the layer is given in Fig. 1.

We assume that the saturated porous medium is isotropic and homogeneous, that the effect of viscous dissipation can be neglected, and that the local thermal non-equilibrium (LTNE) can be described by a two-temperature model [1]. Thus, according to the Oberbeck–Boussinesq approximation, we can write the local mass, momentum and energy balance equations in a dimensionless form as

$$\nabla \cdot \mathbf{u} = 0, \tag{1a}$$

$$\nabla \times \mathbf{u} = \frac{1+\gamma}{\gamma} R \nabla \times \left[T_f(\sin\phi\, \hat{\mathbf{e}}_x + \cos\phi\, \hat{\mathbf{e}}_y)\right], \tag{1b}$$

$$\lambda \frac{\partial T_s}{\partial t} = \nabla^2 T_s + H\gamma(T_f - T_s), \tag{1c}$$

$$\frac{\partial T_f}{\partial t} + \mathbf{u}\cdot\nabla T_f = \nabla^2 T_f + H(T_s - T_f). \tag{1d}$$

The dimensionless quantities employed in Eqs. (1) are defined as

$$(x,y,z) = (x^\star, y^\star, z^\star)\frac{1}{L}, \quad t = t^\star \frac{\alpha_f}{L^2},$$
$$\mathbf{u} = (u,v,w) = (u^\star, v^\star, w^\star)\frac{L}{\chi\alpha_f} = \mathbf{u}^\star \frac{L}{\chi\alpha_f}, \quad T_{s,f} = \frac{T^\star_{s,f} - T_0}{\Delta T}, \tag{2}$$
$$R = \frac{g\beta\Delta T K L}{\alpha_m \nu}, \quad \gamma = \frac{\chi k_f}{(1-\chi)k_s}, \quad \lambda = \frac{\alpha_f}{\alpha_s}, \quad H = \frac{hL^2}{\chi k_f}.$$

Here, the stars denote the dimensional time, coordinates and fields, while the subscripts "s" and "f" denote the solid phase and the fluid phase, respectively. The inter-phase heat transfer coefficient h serves to model the heat exchange between the fluid and the solid phase. We point out that h describes a local volumetric heat transfer

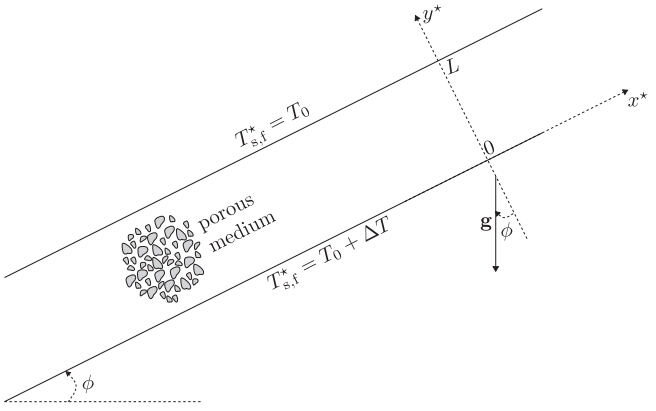

Fig. 1. The fluid saturated porous layer and the thermal boundary conditions.

and, as a consequence, it is expressed in W/(m^3 K) instead of W/(m^2 K) as it usually happens when modelling surface heat transfer.

The four dimensionless parameters, appearing in the governing equations (1) and defined by Eq. (2), are the Darcy-Rayleigh number, R, the conductivity ratio, γ, the diffusivity ratio, λ, and the inter-phase heat transfer parameter, H. We note that the definition of Darcy–Rayleigh number given in Eq. (2) is consistent with that declared under local thermal equilibrium (LTE) conditions. The same definition has been recently employed also by Barletta and Rees [31]. An alternative definition has been proposed, for instance, in Banu and Rees [21]. These authors defined a Darcy-Rayleigh number that coincides with R multiplied by $(1+\gamma)/\gamma$.

Eq. (1b) expresses the local momentum balance including, on the right hand side, the buoyancy force contribution. This equation is obtained by taking the curl of Darcy's law, so that the pressure force term does not appear explicitly.

The boundary conditions on the velocity field and the temperature field are expressed in dimensionless form as

$$\begin{aligned} &y=0: \quad v=0, \quad T_\mathrm{s}=T_\mathrm{f}=1,\\ &y=1: \quad v=0, \quad T_\mathrm{s}=T_\mathrm{f}=0. \end{aligned} \tag{3}$$

3. The single-cell basic flow

A stationary solution of Eqs. (1) can be found such that the velocity field is a parallel vector field directed along the x-axis, and the temperature field depends only on y,

$$\begin{aligned} &u_\mathrm{b}=\frac{1+\gamma}{\gamma}\left(\frac{1}{2}-y\right)R\sin\phi, \quad v_\mathrm{b}=0, \quad w_\mathrm{b}=0,\\ &T_\mathrm{sb}=T_\mathrm{fb}=1-y, \end{aligned} \tag{4}$$

where the subscript "b" stands for "basic solution". Eq. (4) corresponds to a LTE solution. This basic flow with a vanishing mass flow rate is induced by the buoyancy force, and describes a single-cell circulation having an infinite width along the x-direction.

4. Small-amplitude disturbances

The perturbation of the basic velocity and temperature fields Eq. (4) can be expressed as

$$\mathbf{u}=\mathbf{u}_\mathrm{b}+\varepsilon\mathbf{U}, \quad T_\mathrm{s,f}=T_\mathrm{sb,fb}+\varepsilon\Theta_\mathrm{s,f}, \tag{5}$$

where ε is an amplitude parameter. Thus, Eqs. (1) yield the linearised set of equations

$$\nabla\cdot\mathbf{U}=0, \tag{6a}$$

$$\nabla\times\mathbf{U}=\frac{1+\gamma}{\gamma}\,R\,\nabla\times\left[\Theta_\mathrm{f}\left(\sin\phi\;\hat{\mathbf{e}}_x+\cos\phi\;\hat{\mathbf{e}}_y\right)\right], \tag{6b}$$

$$\lambda\,\frac{\partial\Theta_\mathrm{s}}{\partial t}=\nabla^2\Theta_\mathrm{s}+H\gamma(\Theta_\mathrm{f}-\Theta_\mathrm{s}), \tag{6c}$$

$$\frac{\partial\Theta_\mathrm{f}}{\partial t}+\frac{\partial\Theta_\mathrm{f}}{\partial x}\,\frac{1+\gamma}{\gamma}\left(\frac{1}{2}-y\right)R\sin\phi-V=\nabla^2\Theta_\mathrm{f}+H(\Theta_\mathrm{s}-\Theta_\mathrm{f}), \tag{6d}$$

where the terms $\mathrm{O}(\varepsilon^2)$ have been neglected. The boundary conditions for the disturbances, $(\mathbf{U},\Theta)$, are

$$y=0,1: \quad V=0, \quad \Theta_\mathrm{s}=\Theta_\mathrm{f}=0. \tag{7}$$

A pressure representation of the velocity disturbance $\mathbf{U}$,

$$\mathbf{U}=\frac{1+\gamma}{\gamma}\,R\Theta_\mathrm{f}\left(\sin\phi\;\hat{\mathbf{e}}_x+\cos\phi\;\hat{\mathbf{e}}_y\right)-\nabla P \tag{8}$$

allows one to satisfy identically Eq. (6b), and to express the other governing equations (6) and boundary conditions (7) as

$$\nabla^2P=\frac{1+\gamma}{\gamma}\,R\left(\frac{\partial\Theta_\mathrm{f}}{\partial x}\,\sin\phi+\frac{\partial\Theta_\mathrm{f}}{\partial y}\,\cos\phi\right), \tag{9a}$$

$$\lambda\,\frac{\partial\Theta_\mathrm{s}}{\partial t}=\nabla^2\Theta_\mathrm{s}+H\gamma(\Theta_\mathrm{f}-\Theta_\mathrm{s}), \tag{9b}$$

$$\frac{\partial\Theta_\mathrm{f}}{\partial t}+\frac{\partial\Theta_\mathrm{f}}{\partial x}\,\frac{1+\gamma}{\gamma}\left(\frac{1}{2}-y\right)R\sin\phi-\frac{1+\gamma}{\gamma}\,R\Theta_\mathrm{f}\cos\phi+\frac{\partial P}{\partial y}=\nabla^2\Theta_\mathrm{f}+H(\Theta_\mathrm{s}-\Theta_\mathrm{f}), \tag{9c}$$

$$y=0,1: \quad \frac{\partial P}{\partial y}=0, \quad \Theta_\mathrm{s}=\Theta_\mathrm{f}=0. \tag{9d}$$

We now study the normal modes of Eqs. (9) expressed as

$$\left\{\begin{matrix}P(x,y,z,t)\\ \Theta_\mathrm{s,f}(x,y,z,t)\end{matrix}\right\}=\left\{\begin{matrix}p(y)\\ \theta_\mathrm{s,f}(y)\end{matrix}\right\}\exp\left[i(a_xx+a_zz-\omega t)\right], \tag{10}$$

where $a_x\hat{\mathbf{e}}_x+a_z\hat{\mathbf{e}}_z$ is the wave vector, $a=\sqrt{a_x^2+a_z^2}$ is the wave number, and ω is a complex parameter. The real part of ω, $\Re e(\omega)$, is the angular frequency of the wave. The imaginary part, $\Im m(\omega)$, is the exponential growth parameter. If $\Im m(\omega)<0$, the normal mode describes a stability condition. On the other hand, if $\Im m(\omega)>0$, the normal mode yields instability. The breakup of the single-cell flow regime occurs at the marginal stability threshold, namely when $\Im m(\omega)=0$. In the following, we will focus on the marginal stability condition, so that we will tacitly assume $\Im m(\omega)=0$.

General modes with $0\leqslant a_x\leqslant a$ and $0\leqslant a_z\leqslant a$ are termed oblique rolls. The modes with $a_x=a$ and $a_z=0$ are called transverse rolls, while the modes with $a_x=0$ and $a_z=a$ are the longitudinal rolls.

Substitution of Eq. (10) into Eqs. (9) yields

$$p''-a^2p-\frac{1+\gamma}{\gamma}\,R(ia_x\theta_\mathrm{f}\sin\phi+\theta_\mathrm{f}'\cos\phi)=0, \tag{11a}$$

$$\theta_\mathrm{s}''-a^2\theta_\mathrm{s}+H\gamma(\theta_\mathrm{f}-\theta_\mathrm{s})+i\omega\lambda\theta_\mathrm{s}=0, \tag{11b}$$

$$\theta_\mathrm{f}''-a^2\theta_\mathrm{f}+H(\theta_\mathrm{s}-\theta_\mathrm{f})+i\omega\theta_\mathrm{f}-ia_x\theta_\mathrm{f}\,\frac{1+\gamma}{\gamma}\left(\frac{1}{2}-y\right)R\sin\phi+\frac{1+\gamma}{\gamma}\,R\theta_\mathrm{f}\cos\phi-p'=0, \tag{11c}$$

$$y=0,1: \quad p'=0, \quad \theta_\mathrm{s}=\theta_\mathrm{f}=0, \tag{11d}$$

where primes denote the derivatives with respect to y. By employing the same transformation defined by Rees and Bassom [10], the eigenvalue problem Eqs. (11) for arbitrary oblique rolls can be mapped onto an equivalent eigenvalue problem for two-dimensional normal modes with $a_x=a$ and $a_z=0$, *viz.* transverse rolls. More precisely, we can map the pair of parameters (ϕ,R) onto a new pair (Φ,S) such that

$$\left\{\begin{matrix}R\cos\phi=S\cos\Phi,\\ a_xR\sin\phi=aS\sin\Phi.\end{matrix}\right. \tag{12}$$

Eq. (12) implies that Eqs. (11) can be rewritten as

$$p''-a^2p-\frac{1+\gamma}{\gamma}\,S(ia\theta_\mathrm{f}\sin\Phi+\theta_\mathrm{f}'\cos\Phi)=0, \tag{13a}$$

$$\theta_\mathrm{s}''-a^2\theta_\mathrm{s}+H\gamma(\theta_\mathrm{f}-\theta_\mathrm{s})+i\omega\lambda\theta_\mathrm{s}=0, \tag{13b}$$

$$\theta_\mathrm{f}''-a^2\theta_\mathrm{f}+H(\theta_\mathrm{s}-\theta_\mathrm{f})+i\omega\theta_\mathrm{f}-ia\theta_\mathrm{f}\,\frac{1+\gamma}{\gamma}\left(\frac{1}{2}-y\right)S\sin\Phi+\frac{1+\gamma}{\gamma}\,S\theta_\mathrm{f}\cos\Phi-p'=0, \tag{13c}$$

$$y=0,1: \quad p'=0, \quad \theta_\mathrm{s}=\theta_\mathrm{f}=0. \tag{13d}$$

This system of homogeneous differential equations with homogeneous boundary conditions can be solved as an eigenvalue problem to obtain, for prescribed input data (H,γ,λ,Φ), the marginal stability function $S(a)$ and the dispersion relation $\omega(a)$. The minimum of function $S(a)$ defines the critical values a_c and S_c.

5. Longitudinal rolls

If we set $a_x = 0$, Eq. (12) can be solved with

$$\Phi = 0^\circ, \quad S = R\cos\phi. \tag{14}$$

Thus, Eqs. (13) for the longitudinal rolls yield

$$p'' - a^2 p - \frac{1+\gamma}{\gamma} S\theta_f' = 0, \tag{15a}$$

$$\theta_s'' - a^2\theta_s + H\gamma(\theta_f - \theta_s) + i\omega\lambda\theta_s = 0, \tag{15b}$$

$$\theta_f'' - a^2\theta_f + H(\theta_s - \theta_f) + i\omega\theta_f + \frac{1+\gamma}{\gamma} S\theta_f - p' = 0, \tag{15c}$$

$$y = 0, 1: \quad p' = 0, \quad \theta_s = \theta_f = 0. \tag{15d}$$

Since in Eqs. (15) there is no explicit dependence on the inclination angle, the eigenvalue problem for the longitudinal rolls is formally the same as that for the Darcy–Bénard problem in a horizontal layer with LTNE conditions. This problem was solved by Banu and Rees [21]. These authors stated that the eigenvalue problem expressed by Eqs. (15) satisfies the exchange of stabilities, so that $\omega = 0$. A formal proof is given here in Appendix A. Thus, Eqs. (15) can be simplified to

$$p'' - a^2 p - \frac{1+\gamma}{\gamma} S\theta_f' = 0, \tag{16a}$$

$$\theta_s'' - a^2\theta_s + H\gamma(\theta_f - \theta_s) = 0, \tag{16b}$$

$$\theta_f'' - a^2\theta_f + H(\theta_s - \theta_f) + \frac{1+\gamma}{\gamma} S\theta_f - p' = 0, \tag{16c}$$

$$y = 0, 1: \quad p' = 0, \quad \theta_s = \theta_f = 0. \tag{16d}$$

In agreement with Banu and Rees [21], we find that Eqs. (16) can be solved analytically. For the lowest marginal stability mode, we determine the solution by assuming that p is proportional to $\cos(\pi y)$, while θ_s and θ_f are proportional to $\sin(\pi y)$. Hence, Eqs. (16) yield the marginal stability condition

$$S = \frac{\gamma}{1+\gamma}\frac{\left(a^2+\pi^2\right)^2\left(a^2+\pi^2+H+H\gamma\right)}{a^2\left(a^2+\pi^2+H\gamma\right)}. \tag{17}$$

We note that, on account of Eq. (14), the marginal stability condition expressed in terms of the Darcy–Rayleigh number R exploits a dependence on the inclination angle ϕ through a factor $1/\cos\phi$. This conclusion is exactly the same as that drawn for the case of

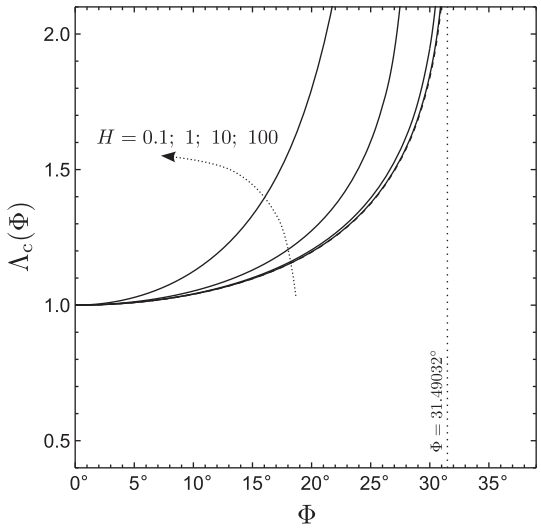

Fig. 2. Case $\gamma \to 0$: plots of $\Lambda_c(\Phi)$ for different values of H; the dashed curve is for $H \to 0$; the dotted vertical line denotes the threshold angle for the existence of transverse rolls when $H \to 0$.

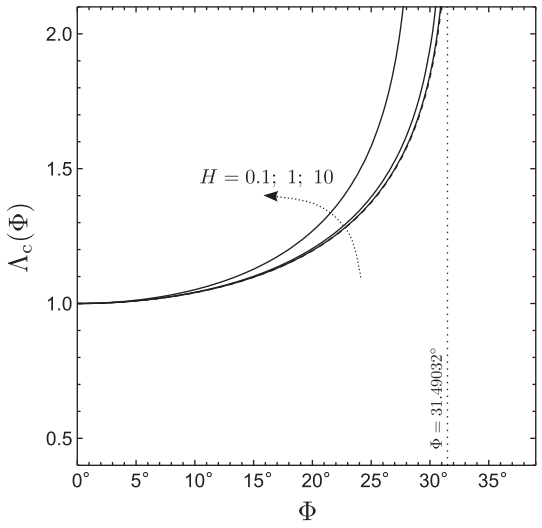

Fig. 3. Case $\gamma = 0.1$: plots of $\Lambda_c(\Phi)$ for different values of H; the dashed curve is for $H \to 0$ and for $H \to \infty$; the dotted vertical line denotes the threshold angle for the existence of transverse rolls in the LTE regime ($H \to \infty$).

LTE and described, for instance, in Nield and Bejan [1]. As a consequence, an increasing inclination to the horizontal implies a stabilizing effect on the basic flow, *viz.* a monotonic increment of the lowest eigenvalue R corresponding to assigned values of (a, H, γ), evaluated through Eqs. (14) and (17).

There are two sensible limiting cases of Eq. (17), $H \to 0$ and $H \to \infty$. The former limit defines the complete thermal uncoupling between the solid phase and the fluid phase, while the latter limit defines the local thermal equilibrium (LTE) between the phases. If $H \to 0$, with $\gamma \sim O(1)$, Eq. (17) yields

$$S = \frac{\gamma}{1+\gamma}\frac{\left(a^2+\pi^2\right)^2}{a^2}. \tag{18}$$

If $H \to \infty$, with $\gamma \sim O(1)$, Eq. (17) yields

$$S = \frac{\left(a^2+\pi^2\right)^2}{a^2}. \tag{19}$$

An important point is that the same limiting expression of $S(a)$ expressed by Eq. (19) is also obtained when $\gamma \to \infty$, with $H \sim O(1)$. In fact, the LTE condition can be also reached with a finite inter-phase heat transfer coefficient provided that $\gamma \gg 1$, *viz.* $\chi k_f \gg (1-\chi)k_s$.

We mention that the neutral stability conditions, Eqs. (18) and (19), for the two opposite regimes $H \to 0$ and $H \to \infty$ just differ by an overall scaling factor, $\gamma/(1+\gamma)$.

In the limiting cases defined above, the critical conditions for the onset of the instability to longitudinal rolls are given by, respectively,

$$\begin{aligned} &a_c = \pi, \quad S_c = \frac{4\pi^2\gamma}{1+\gamma}, \quad \text{when } H \to 0, \text{ with } \gamma \sim O(1), \\ &a_c = \pi, \quad S_c = 4\pi^2, \quad \begin{cases} \text{when } H \to \infty, \text{ with } \gamma \sim O(1) \\ \text{when } \gamma \to \infty, \text{ with } H \sim O(1) \end{cases}. \end{aligned} \tag{20}$$

6. Oblique rolls

If we consider a general angle $\Phi \in [0^\circ, 90^\circ]$, the solution of Eqs. (13) is to be obtained numerically. An efficient and accurate procedure is the combined use of a Runge–Kutta solver and the shooting method. A description is provided in Appendix B.

Several limiting cases can be explored where the general eigenvalue problem, Eqs. (13), is significantly simplified.

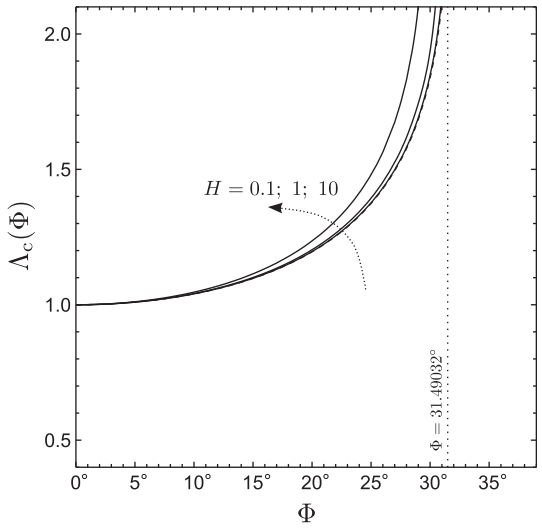

Fig. 4. Case $\gamma = 1$: plots of $\Lambda_c(\Phi)$ for different values of H; the dashed curve is for $H \to 0$ and for $H \to \infty$; the dotted vertical line denotes the threshold angle for the existence of transverse rolls in the LTE regime ($H \to \infty$).

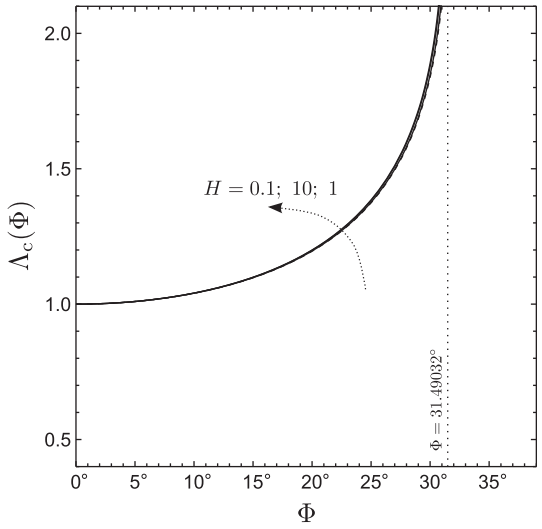

Fig. 5. Case $\gamma = 10$: plots of $\Lambda_c(\Phi)$ for different values of H; the dashed curve is for $H \to 0$ and for $H \to \infty$; the dotted vertical line denotes the threshold angle for the existence of transverse rolls in the LTE regime ($H \to \infty$).

6.1. Limit $H \to 0$, with $\gamma \sim \mathrm{O}(1)$

In this case of complete thermal decoupling between the phases, Eq. (13b) becomes independent of the others. Its unique solution for a general a satisfying the boundary conditions, Eq. (13d), is $\theta_s = 0$. Then, we may reduce Eqs. (13) to a system of two differential equations,

$$p'' - a^2 p - \widetilde{S}\left(ia\theta_f \sin\Phi + \theta_f' \cos\Phi\right) = 0, \tag{21a}$$

$$\theta_f'' - a^2\theta_f + i\omega\theta_f - ia\theta_f\left(\frac{1}{2} - y\right)\widetilde{S}\sin\Phi + \widetilde{S}\theta_f\cos\Phi - p' = 0, \tag{21b}$$

$$y = 0, 1: \quad p' = 0, \quad \theta_f = 0, \tag{21c}$$

where the parameter $\widetilde{S}$ is defined as

$$\widetilde{S} = \frac{1+\gamma}{\gamma}\, S. \tag{22}$$

Eqs. (21) are independent of λ, and depend on γ only implicitly through the parameter $\widetilde{S}$.

6.2. Limit $\gamma \to 0$, with $H \sim \mathrm{O}(1)$

This case corresponds to a condition where $\chi k_f \ll (1-\chi)k_s$. We may infer that Eq. (13b) becomes independent of the others, and that its unique solution for a general a satisfying the boundary conditions, Eq. (13d), is $\theta_s = 0$. If we assume that the parameter $\widetilde{S}$ defined by Eq. (22) is O(1), then Eqs. (13) yield, in the limit $\gamma \to 0$,

$$p'' - a^2 p - \widetilde{S}\left(ia\theta_f \sin\Phi + \theta_f' \cos\Phi\right) = 0, \tag{23a}$$

$$\theta_f'' - a^2\theta_f - H\theta_f + i\omega\theta_f - ia\theta_f\left(\frac{1}{2} - y\right)\widetilde{S}\sin\Phi + \widetilde{S}\theta_f\cos\Phi - p' = 0, \tag{23b}$$

$$y = 0, 1: \quad p' = 0, \quad \theta_f = 0. \tag{23c}$$

Eqs. (23) are independent of λ. We note that, from a purely mathematical viewpoint, Eqs. (21) are just a special case of Eqs. (23) obtained in the limit $H \to 0$.

Proving that $\widetilde{S}(a) \sim \mathrm{O}(1)$, in the limit $\gamma \to 0$, by solving the eigenvalue problem Eqs. (23) implies that $S(a)$ is in fact identically zero for every input data (H, Φ). On inspecting Eq. (17), it is evident that this is the case for longitudinal rolls ($\Phi = 0$), since one has

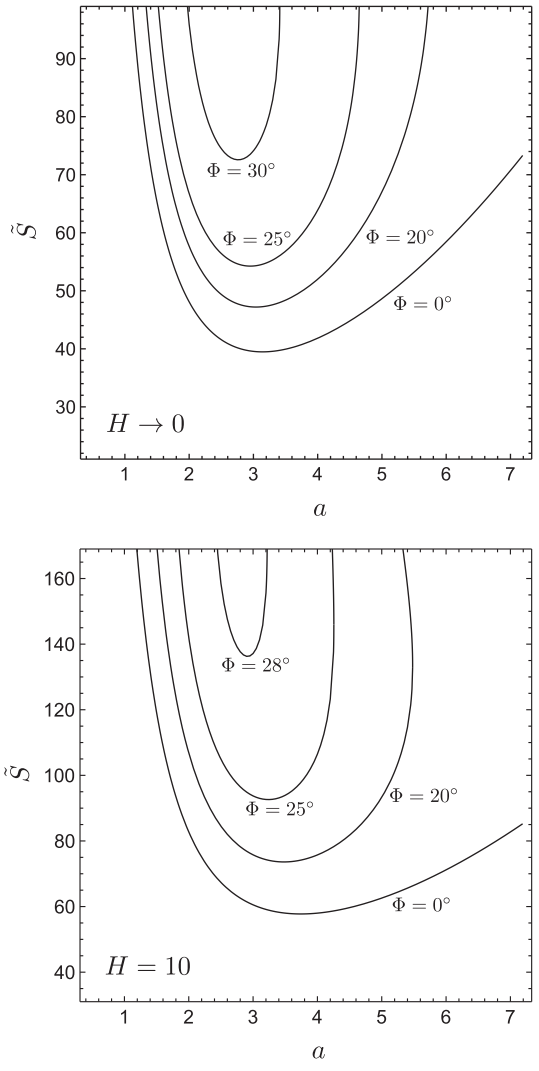

Fig. 6. Case $\gamma \to 0$: neutral stability curves in the $(a, \widetilde{S})$-plane for different angles Φ; the upper frame is for $H \to 0$, while the lower frame is for $H = 10$.

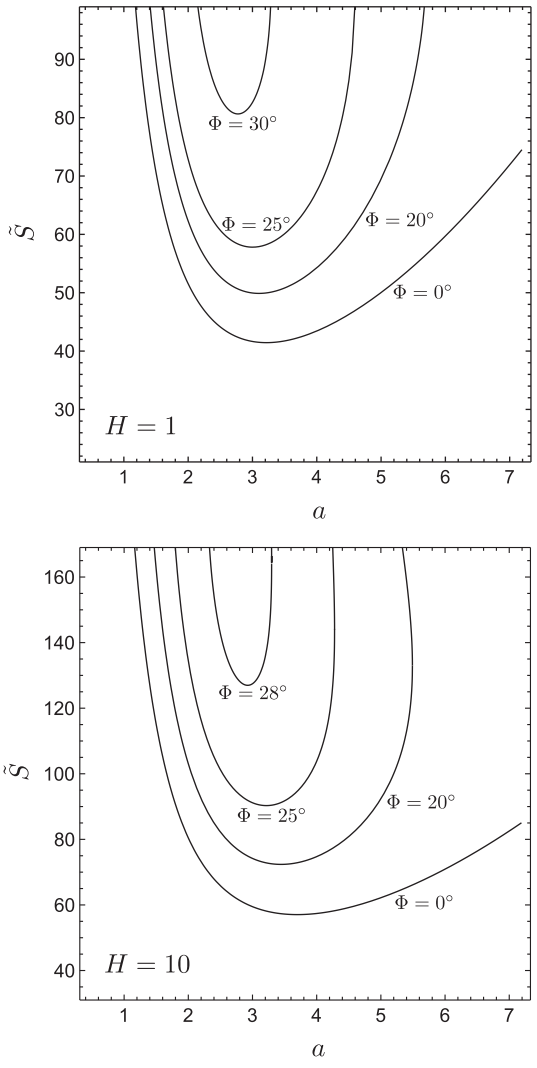

Fig. 7. Case $\gamma = 0.1$: neutral stability curves in the $(a, \widetilde{S})$-plane for different angles Φ; the upper frame is for $H = 1$, while the lower frame is for $H = 10$.

$$\widetilde{S}(a) = \frac{(a^2+\pi^2)(a^2+\pi^2+H)}{a^2}. \tag{24}$$

The minimum of $\widetilde{S}(a)$ defines the critical values for longitudinal rolls that, on account of Eq. (24), are given by

$$a_c = \sqrt{\pi}(H+\pi^2)^{1/4}, \quad \widetilde{S}_c = H + 2\pi\left(\pi + \sqrt{H+\pi^2}\right). \tag{25}$$

6.3. Local thermal equilibrium (LTE)

The LTE condition can be attained by two possible limiting cases,

$$\begin{array}{l} \text{limit } H \to \infty, \quad \text{with } \gamma \sim \mathrm{O}(1); \\ \text{limit } \gamma \to \infty, \quad \text{with } H \sim \mathrm{O}(1). \end{array} \tag{26}$$

We first define

$$\theta = \frac{\theta_s + \gamma\,\theta_f}{\gamma}, \tag{27}$$

so that, by combining Eqs. (13b) and (13c), Eqs. (13) can be rewritten as

$$p'' - a^2 p - \frac{1+\gamma}{\gamma} S\left(ia\,\theta_f \sin\Phi + \theta_f' \cos\Phi\right) = 0, \tag{28a}$$

$$\theta_s'' - a^2\theta_s + H\gamma(\theta_f - \theta_s) + i\omega\lambda\theta_s = 0, \tag{28b}$$

$$\theta'' - a^2\theta + i\omega\,\frac{\lambda\theta_s + \gamma\theta_f}{\gamma} - ia\,\theta_f\,\frac{1+\gamma}{\gamma}\left(\frac{1}{2} - y\right)S\sin\Phi + \frac{1+\gamma}{\gamma}\,S\theta_f\cos\Phi - p' = 0, \tag{28c}$$

$$y = 0, 1: \quad p' = 0, \quad \theta_s = \theta_f = 0. \tag{28d}$$

In both the limiting cases given by Eqs. (26), Eq. (28b) is satisfied only if $\theta_s = \theta_f$. This equality implies that Eqs. (28) can be rewritten as

$$p'' - a^2 p - S(ia\,\theta\sin\Phi + \theta'\cos\Phi) = 0, \tag{29a}$$

$$\theta'' - a^2\theta + i\tilde{\omega}\theta - ia\,\theta\left(\frac{1}{2} - y\right)S\sin\Phi + S\theta\cos\Phi - p' = 0, \tag{29b}$$

$$y = 0, 1: \quad p' = 0, \quad \theta = 0, \tag{29c}$$

where

$$\tilde{\omega} = \begin{cases} \omega\,\dfrac{\lambda+\gamma}{1+\gamma}, & \text{in the limit } H \to \infty, \text{ with } \gamma \sim \mathrm{O}(1); \\ \omega, & \text{in the limit } \gamma \to \infty, \text{ with } H \sim \mathrm{O}(1). \end{cases} \tag{30}$$

We realise immediately that the form of the eigenvalue problem Eqs. (29) coincides with that of the eigenvalue problem Eqs. (21).

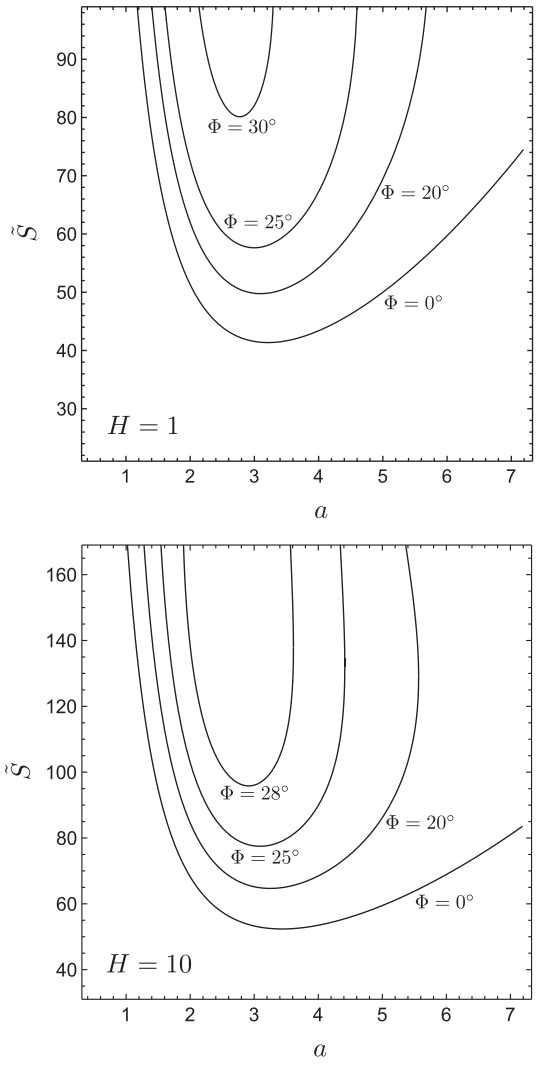

Fig. 8. Case $\gamma = 1$: neutral stability curves in the $(a, \widetilde{S})$-plane for different angles Φ; the upper frame is for $H = 1$, while the lower frame is for $H = 10$.

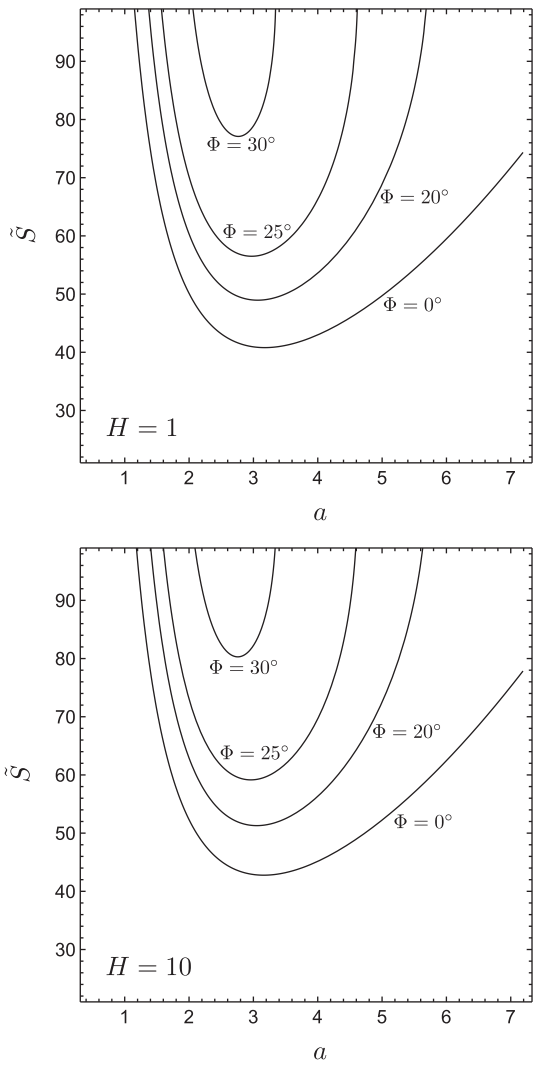

Fig. 9. Case $\gamma = 10$: neutral stability curves in the $(a, \widetilde{S})$-plane for different angles Φ; the upper frame is for $H = 1$, while the lower frame is for $H = 10$.

The two eigenvalue problems can be made identical if, in Eqs. (21), we replace ω with $\tilde{\omega}$, $\widetilde{S}$ with S, and θ_f with θ. This mathematical feature establishes an interesting bridge between two opposite regimes: the limit $H \to 0$ where the two phases are thermally uncoupled, and the limit of LTE.

We mention that the linear stability analysis in the case of LTE was carried out by Rees and Bassom [10] with a streamfunction-temperature formulation instead of a pressure–temperature formulation as in Eqs. (29).

7. Discussion of the results

The analysis of the behaviour of oblique and transverse rolls, as compared to the longitudinal rolls, can be carried out by testing the change of the critical values $(a_c, \widetilde{S}_c)$ when Φ increases above 0°, for prescribed (λ, γ, H). On tracing numerically the evolution of the critical values, $(a_c, \widetilde{S}_c)$, by increasing continuously the angle Φ, the detected oblique rolls display a vanishing angular frequency, $\omega = 0$. The possibility of oblique rolls with $\omega \neq 0$ may arise only for higher modes, not involved in the onset of the instability. The circumstance that we may set $\omega = 0$ in studying the onset of unstable oblique rolls implies that a_c and $\widetilde{S}_c$ are independent of λ. In all cases examined, the oblique rolls $(\Phi > 0°)$ are less unstable than the longitudinal rolls $(\Phi = 0°)$. A convenient way to show up this feature is by plotting, for given values of γ and H, the ratio between $\widetilde{S}_c$ evaluated for $\Phi > 0°$ and $\widetilde{S}_c$ evaluated for $\Phi = 0°$,

$$\Lambda_c(\Phi) = \frac{\widetilde{S}_{c,\Phi}}{\widetilde{S}_{c,0°}} = \frac{S_{c,\Phi}}{S_{c,0°}}. \tag{31}$$

What we obtain is that $\Lambda_c(\Phi) > 1$ for $\Phi > 0°$, in all the cases examined. The behaviour of the oblique and transverse rolls depends on the pair of input parameters (γ, H). The plots of $\Lambda_c(\Phi)$ reported in Figs. 2–5 are for assigned values of γ. The cases $\gamma \to 0, \gamma = 0.1, 1, 10$ are considered. Each figure displays different curves relative to different values of H.

We note that, for every assigned value of γ, the definition of $\Lambda_c(\Phi)$, Eq. (31), ensures that this function is identical in the two opposite regimes: $H \to 0$, described by the solution of Eqs. (21), and $H \to \infty$, described by the solution of Eqs. (29). These two regimes are denoted in Figs. 3–5 by a dashed curve. In Fig. 2, relative to the case $\gamma \to 0$, the dashed curve describes only the limit $H \to 0$, as the LTE limit $H \to \infty$ is ill-defined in this case. It can be immediately recognised on inspecting Figs. 2–5 that the value of the parameter H becomes less and less important as γ increases, and its influence becomes practically immaterial when $\gamma = 10$ (Fig. 5) or larger. As we anticipated above, Figs. 2–5 show that $\Lambda_c(\Phi) > 1$ whenever $\Phi > 0°$, and this implies that the most unstable modes are always the longitudinal rolls $(\Phi = 0°)$. The function $\Lambda_c(\Phi)$ increases monotonically and, close to the threshold $\Phi = 31.49032°$, it becomes very steep. In fact, $\Phi = 31.49032°$ is a vertical asymptote of $\Lambda_c(\Phi)$ in the limit of LTE $(H \to \infty)$, as it was shown by Rees and Bassom [10]. Physically, this means that no unstable normal modes are found with $\Phi > 31.49032°$ in the limit of LTE. Figs. 2–5 reveal that this statement holds also for the LTNE regime, as all graphs of function $\Lambda_c(\Phi)$ for a finite nonvanishing H lay on the left of the graph for the limiting case $H \to \infty$ (dashed curve). Finally, we note that increasing H from 0 to ∞ means that the graph of $\Lambda_c(\Phi)$ first moves to the left and then to the right in order to match the dashed curve in both the limiting cases $H \to 0$ and $H \to \infty$. It is evident in Figs. 2–5 that the graph with $H = 0.1$ is always almost overlapped to that for $H \to 0$ (or ∞), namely the dashed curve.

The neutral stability curves in the parametric plane $(a, \widetilde{S})$ are drawn, for increasing values of Φ, in Figs. 6–9. Each figure refers to a given γ, increasing from 0 to 10, and each frame is for a prescribed H. These figures show that the lowest neutral stability curve is that for $\Phi = 0°$ (longitudinal rolls). The curves with increasing angles $\Phi > 0°$ (oblique rolls) move continuously upward, thus describing less unstable modes. We also see that, with a fixed γ, the curves corresponding to a higher H yield higher values of $\widetilde{S}$. In other words, an increasing inter-phase heat transfer results in a stabilisation of the basic single-cell flow. We mention that this feature was recognised by Banu and Rees [21], with reference to a horizontal porous layer. Fig. 9 illustrates the behaviour already observed in Fig. 5: when γ is large, the influence of the parameter H is definitely a minor one, since a condition close to LTE is approached.

As anticipated in Section 6.2, Fig. 6 suggests that $\widetilde{S}(a) \sim O(1)$, in the limit $\gamma \to 0$, and this implies that $S(a)$ is identically zero in this limit.

8. A neat example

The Squire-like transformation, Eq. (12), is extremely useful in order to map arbitrary oblique rolls, with wave vector $a_x \hat{\mathbf{e}}_x + a_z \hat{\mathbf{e}}_z$, onto transverse rolls, with $a_z = 0$. This transformation allows us to trace the change of a_x from 0 to $a = \sqrt{a_x^2 + a_z^2}$ by increasing the angle Φ from 0°, meaning $a_x = 0$ (longitudinal rolls), to ϕ, meaning $a_x = a$ (transverse rolls). However, the use of this transformation, as well as the use of S and $\widetilde{S}$ instead of R, makes

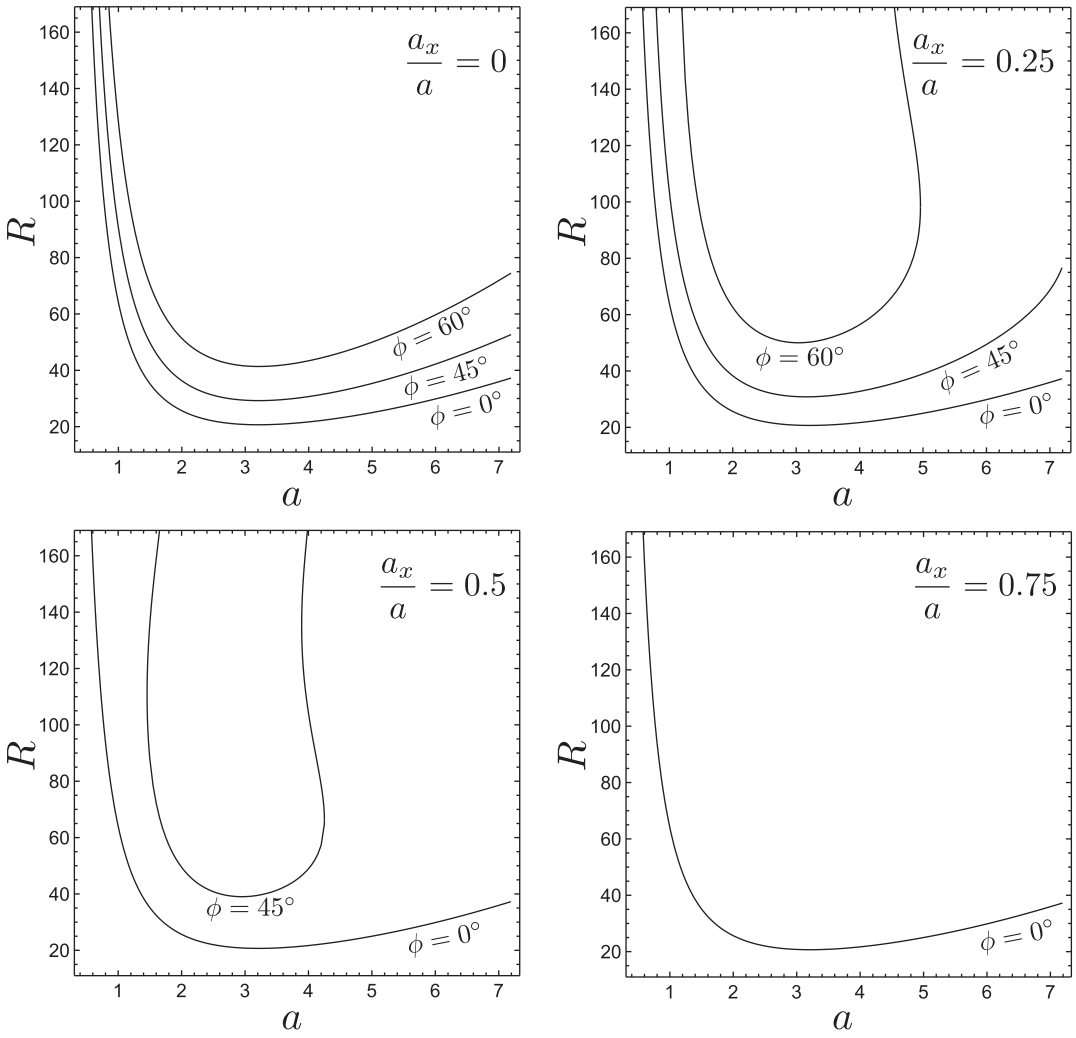

Fig. 10. Case $\gamma = 1, H = 1$: neutral stability curves in the (a, R)-plane for different inclination angles ϕ; each frame corresponds to a different ratio a_x/a.

the physical interpretation of the results a bit cumbersome. Thus, a neat example where the neutral stability curves in the parametric plane $(a, \widetilde{S})$, with increasing Φ, are illustrated in the anti-transformed parametric plane (a, R), with increasing a_x/a, may be useful. To this end, we refer to the case $\gamma = 1$, $H = 1$ (upper frame of Fig. 8).

Fig. 10 shows the change of the neutral stability curves in the (a, R)-plane for three tilt angles, $\phi = 0°$, $45°$, $60°$, as the ratio a_x/a increases above 0. An increasing ratio a_x/a means an increasing inclination of the wave vector to the z-axis, and hence a progressive departure from the longitudinal rolls. The neutral stability curve relative to $\phi = 0°$ is not affected by the value of a_x/a. In fact, when the porous layer is horizontal ($\phi = 0°$), the oblique rolls are equivalent to the longitudinal rolls as the system is invariant by rotations around the vertical axis. As a_x/a increases, the neutral stability curves with $\phi = 45°$ and $60°$ move upwards and eventually disappear. The neutral stability curve with $\phi = 60°$ disappears when a_x/a increases from 0.25 to 0.5. The neutral stability curves with $\phi = 45°$ disappears when a_x/a increases from 0.5 to 0.75. The reason why the neutral stability curves with $\phi = 45°$ and $60°$ disappear may be inferred from Fig. 4. In fact, if $\phi = 60°$ and $a_x/a = 0.5$, Eq. (12) implies that $\Phi = 40.8934°$, namely a value where the instability to oblique rolls is not allowed, as it is deduced by inspecting Fig. 4. By the same reasoning, we exclude also the possibility of instability to oblique rolls with $\phi = 45°$ and $a_x/a = 0.75$; in fact, Eq. (12) implies that $\Phi = 36.8699°$ in this case.

9. Conclusions

The stability of the basic stationary single-cell flow in an inclined porous layer saturated by a fluid has been studied in a regime of local thermal non-equilibrium (LTNE). The LTNE regime has been modelled by a two-temperature scheme employing a finite inter-phase heat transfer coefficient. The characteristic dimensionless parameter of LTNE is H, with $H \to 0$ meaning a complete thermal decoupling between the phases, and $H \to \infty$ leading to a condition of local thermal equilibrium (LTE). Another important dimensionless parameter is the thermal conductivity ratio γ, where $\gamma \to 0$ models a medium with a solid phase much more conductive than the fluid phase, and $\gamma \to \infty$ leads to a LTE condition even if H is finite. We mention that the limit $\gamma \to 0$ may have a special interest when studying the behaviour of porous media such as the metallic foams.

The response to small-amplitude linear disturbances has been tested by adopting a normal mode analysis. Normal modes with an arbitrary inclination of the wave vector have been considered, *viz.* oblique rolls, including longitudinal rolls (wave vector perpendicular to the basic velocity) and transverse rolls (wave vector parallel to the basic velocity) as special cases. The exchange of stabilities has been proved for the longitudinal rolls. A Squire-like transformation has been adopted to map all the oblique rolls onto corresponding transverse rolls. Accordingly the tilt angle of the layer, ϕ, has been replaced with a transformed angle Φ, and the

Darcy–Rayleigh number R has been replaced with a transformed Darcy–Rayleigh number S.

The neutral stability curves and the critical values of the Darcy-Rayleigh number have been obtained for different choices of the governing parameters (Φ, γ, H). The study was carried out with a numerical solution of the eigenvalue problem, based on a combined Runge–Kutta solver and shooting method. The analysis allowed us to deduce the following.

(a) The longitudinal rolls are the most unstable normal modes. This instability exists for every tilt angle ϕ smaller than 90°. At neutral stability, the Darcy–Rayleigh number depends on ϕ through a cosine factor, thus allowing a simple correspondence to the neutral stability threshold for a horizontal layer. The LTNE condition implies that the instability to longitudinal rolls is enhanced with respect to the asymptotic LTE regime.

(b) The oblique and transverse rolls are unstable only for sufficiently small tilt angles. The upper bound, $\phi = 31.49032°$, for the existence of transverse roll instability under LTE conditions (see Rees and Bassom [10]) is not exceeded in the LTNE regime. Higher branches of travelling oblique modes may exist, but they have been disregarded in this analysis as they have no relevance to the onset of the instability.

The above described stability analysis was carried out by modelling the heating from below through a pair of isothermal and impermeable boundary planes. An opportunity for future developments of this research is the study of different models for the temperature boundary conditions. This task is specially challenging if uniform heat flux at a boundary is assumed. This type of boundary conditions require a non-trivial modelling in the LTNE regime as it was pointed out, for instance, by Amiri et al. [17], Alazmi and Vafai [20], Yang and Vafai [28], Barletta and Rees [31].

Conflict of interest

None declared.

Acknowledgement

This work has been financially supported by Alma Mater Studiorum Università di Bologna.

Appendix A. Exchange of stabilities

It can be proved by an integral method [32,33] that the exchange of stabilities holds for Eqs. (15), namely that only non-travelling ($\omega = 0$) longitudinal modes are allowed. In the following, we denote by an overline the complex conjugate of a function. On multiplying Eq. (15b) by $\bar{\theta}_s$, integrating with respect to y in the interval $0 \leqslant y \leqslant 1$, using the integration by parts wherever needed, and simplifying according to the boundary conditions, Eq. (15d), we obtain

$$-\int_0^1 \left(|\theta_s'|^2 + a^2|\theta_s|^2\right)dy + H\gamma\left(\int_0^1 \bar{\theta}_s\theta_f\,dy - \int_0^1 |\theta_s|^2 dy\right) + i\omega\lambda\int_0^1 |\theta_s|^2 dy = 0. \tag{A1}$$

Then, we multiply Eq. (15c) by $\bar{\theta}_f$, integrate with respect to y in the interval $0 \leqslant y \leqslant 1$, and simplify according to the integration by parts with the boundary conditions, Eq. (15d),

$$-\int_0^1 \left(|\theta_f'|^2 + a^2|\theta_f|^2\right)dy + H\left(\int_0^1 \bar{\theta}_f\theta_s\,dy - \int_0^1 |\theta_f|^2 dy\right) + i\omega\int_0^1 |\theta_f|^2 dy + \frac{1+\gamma}{\gamma}\,S\int_0^1 |\theta_f|^2 dy + \int_0^1 \bar{\theta}_f' p\,dy = 0. \tag{A2}$$

From Eqs. (15a) and (15d), one obtains the integral equation

$$\frac{1+\gamma}{\gamma}\,S\int_0^1 \bar{\theta}_f' p\,dy = -\int_0^1 \left(|p'|^2 + a^2|p|^2\right)dy, \tag{A3}$$

so that Eq. (A2) can be rewritten as

$$-\int_0^1 \left(|\theta_f'|^2 + a^2|\theta_f|^2\right)dy + H\left(\int_0^1 \bar{\theta}_f\theta_s\,dy - \int_0^1 |\theta_f|^2 dy\right) + i\omega\int_0^1 |\theta_f|^2 dy + \frac{1+\gamma}{\gamma}\,S\int_0^1 |\theta_f|^2 dy - \frac{\gamma}{(1+\gamma)S}\int_0^1 \left(|p'|^2 + a^2|p|^2\right)dy = 0. \tag{A4}$$

We now multiply Eq. (A4) by γ and sum Eqs. (A1) and (A4), so that we obtain

$$-\int_0^1 \left[\gamma|\theta_f'|^2 + |\theta_s'|^2 + a^2\left(\gamma|\theta_f|^2 + |\theta_s|^2\right)\right]dy + H\gamma\left[2\int_0^1 \Re e(\bar{\theta}_f\theta_s)\,dy - \int_0^1 \left(|\theta_f|^2 + |\theta_s|^2\right)dy\right] + i\omega\int_0^1 \left(\gamma|\theta_f|^2 + \lambda|\theta_s|^2\right)dy + (1+\gamma)S\int_0^1 |\theta_f|^2 dy - \frac{\gamma^2}{(1+\gamma)S}\int_0^1 \left(|p'|^2 + a^2|p|^2\right)dy = 0. \tag{A5}$$

Eq. (A5) is satisfied if both the real part and the imaginary part of the left hand side are zero. In particular, if we set the imaginary part to zero, we obtain

$$\omega\int_0^1 \left(\gamma|\theta_f|^2 + \lambda|\theta_s|^2\right)dy = 0. \tag{A6}$$

Since the trivial solution of the eigenvalue problem Eqs. (15) is to be excluded, and both γ and λ are positive, Eq. (A6) holds if and only if $\omega = 0$. This proves that the exchange of stabilities is satisfied for Eqs. (15).

Appendix B. Numerical solution

The eigenvalue problem defined by Eqs. (13) can be solved numerically by employing a fourth-order Runge–Kutta solver combined with the shooting method. To this end, we first reformulate Eqs. (13) as an initial value problem, by completing artificially the conditions at $y = 0$, namely

$$y = 0: \quad \begin{matrix} p = 1, & p' = 0, \\ \theta_s = 0, & \theta_s' = \eta_1 + i\eta_2, \\ \theta_f = 0, & \theta_f' = \eta_3 + i\eta_4. \end{matrix} \tag{B1}$$

Since the differential problem defined by Eqs. (13) is homogeneous, the condition $p(0) = 1$ serves for fixing the otherwise arbitrary scale of the solutions (p, θ_s, θ_f). The four real parameters $\eta_{1\ldots4}$ are unknown a priori. They can be determined by the shooting method, through the following scheme:

1. Prescribe the values of $(a, H, \gamma, \lambda, \Phi)$.
2. Solve numerically the initial value problem given by Eqs. (13a)–(13c) and (B1).
3. Use the final conditions at $y = 1$ expressed by Eq. (13d) to determine the unknown real parameters $(\omega, S, \eta_1, \eta_2, \eta_3, \eta_4)$.

In this regard, we note that the final conditions $p'(1) = 0$, $\theta_s(1) = 0$ and $\theta_f(1) = 0$ are complex, so that they yield six real

equations in the six real unknowns $(\omega, S, \eta_1, \eta_2, \eta_3, \eta_4)$. The Runge–Kutta solution of the initial value problem is achieved by means of the function `NDSolve` available in the *Mathematica 10* environment (© Wolfram, Inc.), while the shooting method can be managed, in the same environment, by using the function `FindRoot`.

References

[1] D.A. Nield, A. Bejan, Convection in Porous Media, third ed., Springer, New York, 2006.
[2] D.A.S. Rees, The stability of Darcy–Bénard convection, in: K. Vafai, H.A. Hadim (Eds.), Handbook of Porous Media, CRC Press, New York, 2000, pp. 521–558. Ch. 12.
[3] P.A. Tyvand, Onset of Rayleigh–Bénard convection in porous bodies, in: D.B. Ingham, I. Pop (Eds.), Transport Phenomena in Porous Media II, Pergamon, New York, 2002, pp. 82–112. Ch. 4.
[4] A. Barletta, Thermal instabilities in a fluid saturated porous medium, in: A. Öchsner, G.E. Murch (Eds.), Heat Transfer in Multi-Phase Materials, Springer, New York, 2011, pp. 381–414.
[5] S.A. Bories, M.A. Combarnous, Natural convection in a sloping porous layer, J. Fluid Mech. 57 (1973) 63–79.
[6] J.E. Weber, Thermal convection in a tilted porous layer, Int. J. Heat Mass Transfer 18 (1975) 474–475.
[7] J.P. Caltagirone, S. Bories, Solutions and stability criteria of natural convective flow in an inclined porous layer, J. Fluid Mech. 155 (1985) 267–287.
[8] L. Storesletten, M. Tveitereid, Onset of convection in an inclined porous layer with anisotropic permeability, Appl. Mech. Eng. 4 (1999) 575–587.
[9] M. Karimi-Fard, M.C. Charrier-Mojtabi, A. Mojtabi, Onset of stationary and oscillatory convection in a tilted porous cavity saturated with a binary fluid: linear stability analysis, Phys. Fluids 11 (1999) 1346–1358.
[10] D.A.S. Rees, A.P. Bassom, Onset of Darcy–Bénard convection in an inclined layer heated from below, Acta Mech. 144 (2000) 103–118.
[11] D.A.S. Rees, L. Storesletten, A. Postelnicu, The onset of convection in an inclined anisotropic porous layer with oblique principle axes, Transp. Porous Media 62 (2006) 139–156.
[12] D.A. Nield, A note on convection patterns in an inclined porous layer, Transp. Porous Media 86 (2011) 23–25.
[13] D.A. Nield, A. Barletta, M. Celli, The effect of viscous dissipation on the onset of convection in an inclined porous layer, J. Fluid Mech. 679 (2011) 544–558.
[14] A. Barletta, L. Storesletten, Thermoconvective instabilities in an inclined porous channel heated from below, Int. J. Heat Mass Transfer 54 (2011) 2724–2733.
[15] D.A.S. Rees, A. Barletta, Linear instability of the isoflux Darcy–Bénard problem in an inclined porous layer, Transp. Porous Media 87 (2011) 665–678.
[16] M. Combarnous, S. Bories, Modelisation de la convection naturelle au sein d'une couche poreuse horizontale a l'aide d'un coefficient de transfert solide–fluide, Int. J. Heat Mass Transfer 17 (1974) 505–515.
[17] A. Amiri, K. Vafai, T.M. Kuzay, Effect of boundary conditions on non-Darcian heat transfer through porous media and experimental comparisons, Numer. Heat Transfer A 27 (1995) 651–664.
[18] D.A. Nield, Effects of local thermal non-equilibrium in steady convective processes in a saturated porous medium: forced convection in a channel, J. Porous Media 1 (1998) 181–186.
[19] A.V. Kuznetsov, Thermal nonequilibrium forced convection in porous media, in: D.B. Ingham, I. Pop (Eds.), Transport Phenomena in Porous Media, Pergamon, Oxford, 1998, pp. 103–129.
[20] B. Alazmi, K. Vafai, Constant wall heat flux boundary conditions in porous media under local thermal non-equilibrium conditions, Int. J. Heat Mass Transfer 45 (2002) 3071–3087.
[21] N. Banu, D.A.S. Rees, Onset of Darcy–Bénard convection using a thermal non-equilibrium model, Int. J. Heat Mass Transfer 45 (2002) 2221–2228.
[22] A. Postelnicu, D.A.S. Rees, The onset of Darcy–Brinkman convection in a porous layer using a thermal nonequilibrium model – Part I: Stress-free boundaries, Int. J. Energy Res. 27 (2003) 961–973.
[23] D.A.S. Rees, I. Pop, Local thermal non-equilibrium in porous medium convection, in: D.B. Ingham, I. Pop (Eds.), Transport Phenomena in Porous Media III, Pergamon, Oxford, 2005, pp. 147–173.
[24] A. Postelnicu, Effect of inertia on the onset of mixed convection in a porous layer using a thermal nonequilibrium model, J. Porous Media 10 (2007) 515–524.
[25] A. Nouri-Borujerdi, A.R. Noghrehabadi, D.A.S. Rees, The effect of local thermal non-equilibrium on conduction in porous channels with a uniform heat source, Transp. Porous Media 69 (2007) 281–288.
[26] A. Nouri-Borujerdi, A.R. Noghrehabadi, D.A.S. Rees, Onset of convection in a horizontal porous channel with uniform heat generation using a thermal nonequilibrium model, Transp. Porous Media 69 (2007) 343–357.
[27] A. Postelnicu, The onset of a Darcy–Brinkman convection using a thermal nonequilibrium model. Part II, Int. J. Therm. Sci. 47 (2008) 1587–1594.
[28] K. Yang, K. Vafai, Analysis of temperature gradient bifurcation in porous media – an exact solution, Int. J. Heat Mass Transfer 53 (2010) 4316–4325.
[29] A. Postelnicu, The effect of a horizontal pressure gradient on the onset of a Darcy–Bénard convection in thermal non-equilibrium conditions, Int. J. Heat Mass Transfer 53 (2010) 68–75.
[30] D.A.S. Rees, Microscopic modeling of the two-temperature model for conduction in heterogeneous media, J. Porous Media 13 (2010) 125–143.
[31] A. Barletta, D.A.S. Rees, Local thermal non-equilibrium effects in the Darcy–Bénard instability with isoflux boundary conditions, Int. J. Heat Mass Transfer 55 (2012) 384–394.
[32] A. Pellew, R.V. Southwell, On maintained convective motion in a fluid heated from below, Proc. R. Soc. London Ser. A Math. Phys. Sci. 176 (1940) 312–343.
[33] A. Nouri-Borujerdi, A.R. Noghrehabadi, D.A.S. Rees, Influence of Darcy number on the onset of convection in a porous layer with a uniform heat source, Int. J. Therm. Sci. 47 (2008) 1020–1025.